# Journal Name

## COMMUNICATION

# Synthesis of Boron and Phosphorus Codoped All-Inorganic Colloidal Silicon Nanocrystals from Hydrogen Silsesquioxane

Hiroshi Sugimoto,[a] Minoru Fujii[*a] and Kenji Imakita[a]

**We present a new route for mass-production of B and P codoped all-inorganic colloidal Si nanocrystals (NCs) from hydrogen silsesquioxane (HSQ). Codoped Si NCs are grown in glass matrices by annealing mixture solutions of HSQ and dopant acids, and then extracted from the matrices by hydrofluoric acid etching. The free-standing NCs are dispersible in methanol without any surface functionalization processes. The structural analyses suggest the formation of heavily B and P doped hydrophilic shell on the surface of Si NCs. The NCs show efficient size-tunable photoluminescence in the near infrared to visible region.**

Colloidal semiconductor nanocrystals (NCs), often called NC inks, can be a precursor for the formation of semiconductor films by scalable solution-based processes, and thus are considered to be a key material for the production of future large-area optoelectronic devices.[1,2,3,4] In particular, colloidal solutions of Cd and Pb chalcogenide NCs are most intensively studied because of the established production process of size-controlled mono-dispersed NCs. The surface of these NCs is usually functionalized by relatively long molecules to prevent agglomeration by the steric barriers. By employing a ligand exchange process, which exchanges the organic ligands to metal calcogenides, high carrier mobility films are produced from the colloid by solution-based processes.[5,6]

A major concern with Cd and Pb chalcogenide NCs is their toxicity and influence on the environment. A promising environmentally benign alternative of them is Si NCs. Synthesis of colloidal Si NCs has been reported during the past decade and the quality is improving rapidly. One of the widely employed synthesis method is plasma decomposition of silane-group precursors. The group of Kortshagen demonstrated high-yield synthesis of free-standing Si NCs by non-thermal plasma

decomposition of silane and produced electroluminescence devices by a solution-based process.[7] Their NCs showed bright photoluminescence (PL) with the quantum yield of 60%.[8,9] Another method suitable for mass-production of high-quality Si NCs is that using hydrogen silsesquioxane (HSQ) as a precursor.[10,11] HSQ is a polymer consisting of $HSiO_{1.5}$ units and decomposes into Si-NCs and silica matrices by thermal annealing. By etching out the matrices, Si NCs are liberated in solution.[11] This is a vacuum-free process and thus potentially a low-cost synthesis method. In both synthesis routes, NC surface is functionalized by organic molecules to prevent the agglomeration in solution.

A problem of organic functionalization of Si NC surface is deterioration of carrier transport of films due to increased NC to NC distances. To overcome this problem, all-inorganic colloidal Si NCs have been synthesized. It is shown that Cl-terminated Si NCs synthesized by plasma decomposition of $SiCl_4$ are dispersible in polar solvents without organic capping,[12] although they are vulnerable in air exposure and easily aggregate.[13] Dispersion of Si NCs in polar solvents is also achieved by the formation of high B and P concentration shells on the surface.[14,15] The NCs are stable in alcohol for years and the PL is almost insensitive to the environment.[16,17] A drawback of the codoped NCs is the small production rate. Since the formation process of codoped colloidal Si NCs includes a sputtering process, production of large amount of colloidal solutions meeting the requirement of industrial applications is very hard and expensive.

In this Communication, we report a new simple route for mass-production of Si NCs with high B and P concentration shells by extending the process in Refs. [10] and [11]. The process is summarized in Scheme 1. Codoping of B and P is achieved by simple addition of dopant acids ($H_3BO_3$ and $H_3PO_4$) in HSQ solution. Dried mixture of HSQ, $H_3BO_3$ and $H_3PO_4$ are

annealed at temperatures from 900 to 1200°C in N₂ gas, which results in the growth of Si NCs in borophosphosilicate glass (BPSG) matrices. Si NCs are then liberated from the matrices by hydrofluoric acid (HF) etching. Finally, free-standing Si NCs are dispersed in methanol.
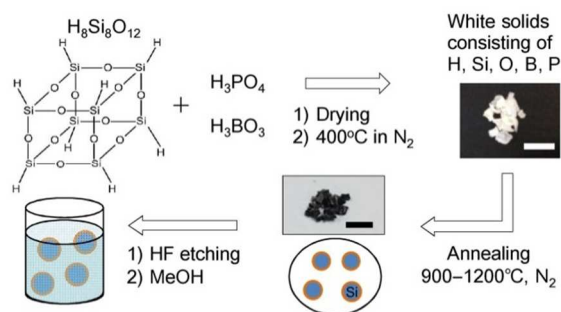


**Scheme 1**. Preparation procedure of all-inorganic B and P codoped colloidal Si NCs. Scale bars in photographs are 1 cm.
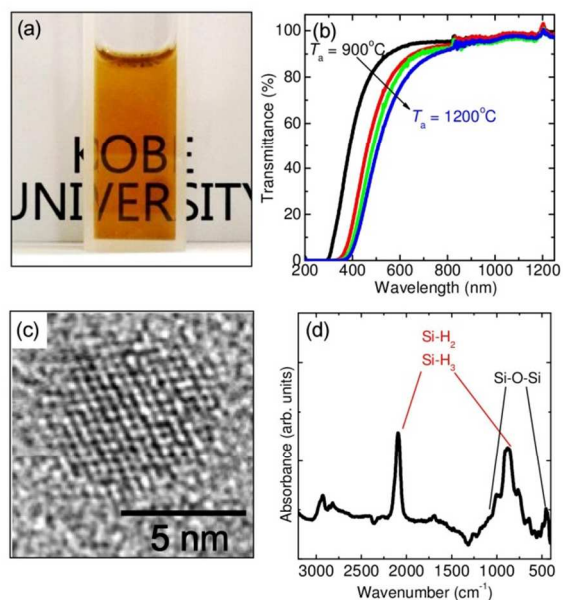


**Figure 1**. (a) Photograph of solution in which codoped Si NCs grown at 1200°C are dispersed. (b) Optical transmittance spectra of solutions containing NCs grown at 900 to 1200°C. (c) High-resolution TEM image of a Si NC grown at 1200 °C. Lattice fringes correspond to (111) plans of Si crystal. (d) IR absorption spectrum of codoped Si NCs grown at 1200°C.

Figures 1(a) shows a picture of a solution of Si NCs grown at 1200°C. The solution is very clear and the characters behind the 1cm cubicle can clearly be seen. The solution is stable and no precipitates are observed for more than 6 months. Optical transmittance spectra of solutions containing NCs grown at 900 to 1200°C are shown in Figure 1(b). The transmittance below the band gap energy of bulk Si crystal is nearly 100%, indicating that light scattering by NC agglomerates is negligibly small. It should be stressed here that Si NCs can be dispersed in methanol only when $H_3BO_3$ and $H_3PO_4$ are simultaneously added in HSQ solution (see Figure S1 in Supporting Information). In the visible range, the absorption onset shifts to the shorter wavelength when the growth temperature is lower.

This is due to smaller sizes and resultant stronger quantum confinement effects for NCs grown at lower temperatures.

Figure 1(c) shows a typical high-resolution TEM image of a Si NC grown at 1200°C. Lattice fringes corresponding to (111) plane of Si crystal (0.31nm) are clearly seen. TEM observations over wide areas reveal that no three-dimensional agglomerates of NCs are formed. This evidences that Si NCs are dispersed in methanol perfectly as isolated NCs. The average diameters and the standard deviations obtained by TEM observations are summarized in Table 1. For NCs grown at 900°C, the size was too small to be estimated by TEM observations.

**Table 1**. List of samples. The annealing temperature ($T_a$), average diameter ($d_{ave}$) and the standard deviation ($\sigma$)

| $T_a$ (°C) | $d_{ave}$ (nm) | $\sigma$ (nm) | B (at.%) | P (at.%) |
|---|---|---|---|---|
| 900 | - | - | 4.5 | 2.4 |
| 1000 | 3.7 | 1.3 | 6.0 | 4.8 |
| 1100 | 4.8 | 1.7 | 8.1 | 4.6 |
| 1200 | 5.3 | 1.7 | 9.0 | 4.1 |

Figure 1(d) shows IR absorption spectrum of Si NCs grown at 1200°C. The peaks around 2100 and 870 cm⁻¹ are due to Si−Hₓ vibrations.[18] The weak peaks around 1080 and 480 cm⁻¹ are assigned to Si−O−Si stretching and rocking vibration modes, respectively. The small peak around 1000 cm⁻¹ is probably due to Oₓ−Si−Hᵧ vibrations.[19,20] The surface of Si NCs are thus hydrogen-terminated and slightly oxidized. No signals assigned to organic molecules such as C−H (~2900 cm⁻¹) and Si−C (680 cm⁻¹) vibrations[21] are observed. This confirms that the high dispersibility of codoped Si NCs in methanol is not due to organic capping, but to other mechanisms.

To analyze the structure of the surface of codoped Si NCs, we measured X-ray photoelectron spectroscopy (XPS) spectra of Si, B and P. In Si 2p spectra in Figure 2(a), a peak appears at 99.8 eV with a tail to the high energy side. The peak is assigned to Si⁰ and is considered to arise from crystalline Si cores.[22] The high-energy tail is from surface native oxide. The tail is larger when the growth temperature is lower. At the lowest temperature (900°C), a sub-peak emerges at 103.8 eV (Si⁴⁺).[22] The increase of the oxides signal at lower growth temperatures can be explained by the increased surface-to-volume ratio. It should be stressed here that, considering the escape depth of photoelectrons, the native oxide is much thinner than 2 nm.[23] This is consistent with the TEM image and the IR absorption spectrum.

In B 1s spectra in Figure 2(b), the peak energy is around 188 eV. It is known that neutral B atoms and $B_2O_3$ exhibit XPS peaks at 187–188 and 193 eV, respectively. Therefore, majority of doped B atoms exist as the non-oxidized states. The situation is similar in P 2p spectra (Figure 2(c)) when the growth temperature is higher than 1000°C. The energy of the peak (130 eV) coincides with P⁰, and thus majority of doped P atoms exist also as the non-oxidized states. When the growth temperature is 900°C, the peak at 135 eV is larger than that of P⁰ at 130 eV.

The 135 eV peak is assigned to $P_2O_5$, indicating that NCs grown at lower temperatures are more vulnerable for oxidation.

In Table 1, B and P concentrations quantified from the integrated peak intensities of XPS spectra are shown. Note that the concentration shown in Table 1 is not the average concentration of a whole volume of a NC, because of the small escape depth of photoelectrons (~2 nm). In small NCs, the concentration may be close to the average concentration, while in large NCs, the concentration of the surface layer is more emphasized and is different from the average concentration. In Table I, the concentration is much higher than the solid solubility limits of B and P in bulk Si crystal.[24] Considering the fact that Si NCs are single crystal with high crystallinity as confirmed by TEM observations, doping of B and P in Si NC cores by exceeding the solubility limits is very unlikely. Therefore, the XPS results indicate that B and P are mainly doped on or near the surface of Si NCs, and heavily B and P doped shells are formed.

Figure 2(d) shows a Raman spectrum of a sample grown at 1200°C. In addition to a Raman peak of crystalline Si at 520 $cm^{-1}$, a broad band is observed around 650 $cm^{-1}$. The band can be assigned to B-related local vibrational modes, such as substitutional B[10] and B[11] and substitutional B-P pairs.[25,26,27] Furthermore, B clusters such as $B_2$ and B-interstitial clusters in crystalline Si lattices exhibit Raman peaks in the 650–700 $cm^{-1}$ range.[28] The observation of the relatively strong 650 $cm^{-1}$ band suggests that the heavily B and P doped shells are crystalline shells.

The TEM, FT-IR, XPS and Raman results suggest the structural model shown in Fig. 2(e). The NC core is B and P doped crystalline Si. The shell is also crystalline Si, but B and P are doped much more heavily, exceeding the solid solubility limit in bulk Si crystal. The outer surface is terminated by hydrogen and oxygen.

Recently, Guerra et al. studied the arrangements of B and P in codoped Si NCs by *ab initio* calculations.[29] They found that pairs of B and P are preferentially located near the surface of NCs. This is consistent with our model that heavily B and P doped crystalline shells are formed. Furthermore, they studied the relative arrangement of B and P. The most energetically favoured structure is that B is located on the outer surface and P in the inner of B.[29]

In bulk Si crystal, it is known that saturated B-rich layers (BRL) are formed at the interface between $B_2O_3$ and Si, when B is heavily-doped by solid state diffusion processes.[30] The BRL is hydrophilic and has high resistance to HF etching.[31] The heavily B and P doped shells in the present Si NCs are considered to be a kind of BRL, which makes Si NCs hydrophilic and dispersible in polar solvents. The difference between B-doped bulk Si crystal and present Si NCs is the necessity of P codoping for the formation of BRL. A possible explanation is that P plays a role to stabilize larger amounts of B atoms at the surface of Si NCs by charge compensation. In fact, theoretical work demonstrates that B and P codoping is energetically much more favourable, and codoped Si NCs have lower formation energy than B or P singly doped ones.[29,32]
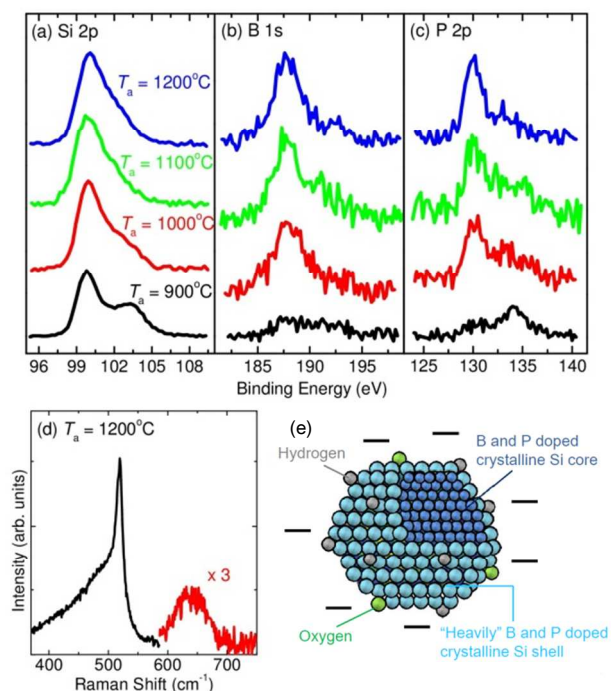


**Figure 2**. XPS spectra of samples grown at 900 to 1200°C (a) Si 2p (b) P 2p (c) B 1s. (d) Raman spectrum of codoped Si NCs grown at 1200°C. (e) Schematic illustration of structural model.
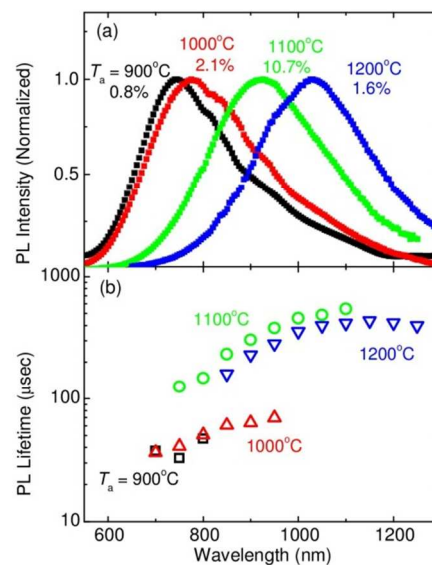


**Figure 3**.(a) Normalized PL spectra of solutions containing codoped Si NCs grown at 900 to 1200°C. PL quantum yields are shown in the figure. (b) PL lifetimes as a function of detection energy.

Figure 3(a) shows PL spectra of codoped colloidal Si NCs. The PL peak shifts from 1030 to 740 nm with decreasing the growth temperature. This is due to stronger confinement of carriers with decreasing the size. In our previous work on codoped colloidal Si NCs prepared by sputtering, we studied the size dependence of the PL properties in detail.[16,33,34] The PL energy of codoped Si NCs is controlled in a very wide range (0.85 - 1.8 eV) by varying the size from 1 nm to 14 nm. In the

whole size range, the PL energy is 300–400 meV lower than that of undoped Si NCs. The consistent low-energy shift of the PL by codoping suggests that the PL arises from the optical transitions between donor and acceptor states (see Figure S2 in Supporting Information).[16,33,34] Since the structure of the present Si NCs is similar to those of the previous work, the PL is also considered to arise from the donor to acceptor transitions. In fact, in Figure 3(a), the low energy tail of the PL spectra of NCs grown at high temperatures extends below the bulk Si band gap. This is evidence that donor and acceptor states contribute to the PL. The quantum yields (QYs) of the PL are shown in the figure. The largest value is 10.7% for NCs grown at 1100$^{\circ}$C.

In Figure 3(b), PL mean lifetimes defined by $\tau = \int_{t_0}^{\infty} \left[\frac{I(t)}{I_0}\right] dt$, where I(t) is the PL intensity as a function of time t and $I_0$ is the initial intensity at time $t_0$, are plotted as a function of the detection wavelength.[35] PL decay curves are shown in Supporting Information (Figure S3). The decay curves are not a single-exponential function. For Si NCs grown at 1100 and 1200$^{\circ}$C, the lifetimes are several hundreds of µs, and are almost independent of the growth temperature, i.e., the lifetime depends only on the detection wavelength. However, the QY of NCs grown at 1200$^{\circ}$C is much smaller than that grown at 1100$^{\circ}$C. This discrepancy suggests that the QY is mainly determined by the number of dark NCs that do not contribute to the PL. Similar scenario can be applied for NCs grown at 900 and 1000$^{\circ}$C. On the other hand, the large difference of the lifetime between the two groups, i.e., NCs grown at 900 and 1000 $^{\circ}$C and those at 1100 and 1200 $^{\circ}$C, is not clear. It may be possible that crystallinity is degraded when the growth temperature is below 1000$^{\circ}$C and the degradation shortens the lifetime.
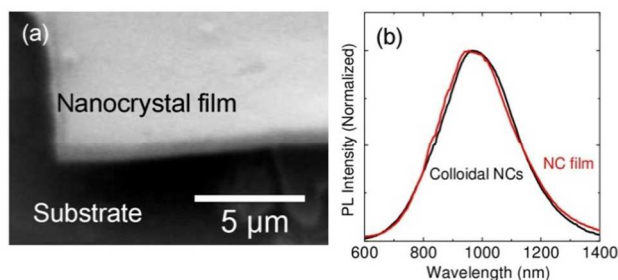


**Figure 4**.(a) SEM image of a NC film prepared by spin-coating colloidal solution containing codoped Si NCs grown at 1200$^{\circ}$C. (b) PL spectrum of codoped colloidal Si NCs and that of the film prepared from the colloid.

Figure 4(a) shows a SEM image of a NC film prepared by spin-coating (1000 rpm, 2 min) concentrated colloid of NCs grown at 1200$^{\circ}$C (~5 mg/ml). A uniform film about 500 nm in thickness is prepared by one spin-coating process. Because of perfect dispersion of isolated NCs in solution, the film is very smooth and flat over a large area. The PL spectrum of the NC film is shown in Fig. 4(b). For comparison, PL spectrum of the colloid is also shown. The spectra are almost identical, indicating that codoped Si-NCs are very stable even after air exposure.

## Conclusions

We developed a novel vacuum-free route for mass-production of all-inorganic colloidal Si NCs. The NCs have heavily B and P doped crystalline shells and the shells make Si NCs hydrophilic and dispersible in polar solvents. The colloids show efficient size-tunable PL in the near IR to visible region. Because of perfect dispersion of isolated Si NCs in solution, smooth and flat NC films are easily prepared by spin-coating the solution.

## Experimental Section

*Synthesis of colloidal Si NCs:* Phosphoric acid solution (100 µL) (85 wt% in ethanol, Wako) and boric acid powder (150 mg) (Wako) were dissolved in 5 mL of ethanol. 400 µL of the solution was added to 1 mL of HSQ (Fox-16, Dow Corning Corporation, 16 wt.% HSQ in methyl isobutyl ketone) solution. The mixture solution was stirred for 30 minutes and dried overnight. The resulting white glassy solid was annealed in $N_2$ gas atmosphere first at 400$^{\circ}$C for 30 min, and then at higher temperatures (900, 1000, 1100 and 1200°C) for 30 min. During the second stage of annealing, the glassy solid transforms into a black lump, which is composed of BPSG containing B and P codoped Si NCs. The size of NCs can be controlled by annealing temperature. Doping concentration can be varied by changing the amount of phosphoric and boric acids in HSQ solution. In order to isolate Si NCs from BPSG matrices, the black lump was ground in a mortar and dissolved in HF solution (46 wt%). Si NCs isolated in HF solution were then transferred to methanol. A large fraction of Si NCs dispersed in methanol without any additional processes and the others precipitated. Precipitates were removed by centrifugation (4500 rpm, 10 min) and the supernatant solutions were stored in a vial. All the processes were performed in an ordinary laboratory environment.

The yield of colloidal Si NCs depends on several parameters such as doping concentration and growth temperature. A yield when HSQ, $H_3PO_4$ and $H_3BO_3$ are 144 mg, 85 mg and 150 mg and the annealing temperature is 1100°C is as follows. By annealing the mixture solution, about 244 mg of BPSG powder containing Si NCs is obtained. The estimated amount of excess Si in the BPSG powder is 16.3 mg. After removing BPSG matrices by HF etching, about 7.3 mg of Si NCs can be retrieved in methanol.

*Characterization*: TEM observations (JEM-2100F, JEOL) were performed for carbon-coated TEM meshes on which colloidal Si NCs are drop-cast. XPS measurements (PHI X-tool, ULVAC-PHI) were carried out using Al K$\alpha$ X-ray source. Raman spectra were measured using a confocal microscope (50× objective lens, NA=0.8) equipped with a single monochromator and a charge coupled device (CCD). The excitation source was a 514.5 nm line of an Ar ion laser. The excitation power was 1.1 mW. The samples for XPS, Raman and IR absorption measurements were prepared by drop-casting colloids on gold-coated Si wafers.

*Photoluminescence measurements*: PL spectra were measured by a spectrofluorometer (Fluorolog-3, HORIBA Jovin Yvon) equipped with a photomultiplier (500−850 nm) and an InGaAs photodiode (800−1300 nm) as detectors. The PL spectra obtained by two different detectors are merged after corrected the sensitivity. The correction factors were obtained by measuring the reference spectrum of a standard halogen lamp. The excitation source was a 405 nm from a monochromatized Xe lamp. The PL QY was determined by a comparative method.[36] Rhodamine 6G in water with a QY of 95% was used as a reference solution. The QY of a sample ($Q_S$) is calculated from PL spectra of reference and colloidal Si NC samples obtained in the same condition using, $Q_S = Q_R (I_S \times A_R \times n_S^2)/(I_R \times A_S \times n_R^2)$, where $Q$ is the quantum yield, $I$ is the integrated PL intensity, $A$ is the absorbance, and $n$ is the refractive index. The subscript S and R refer to the sample and the reference solutions, respectively. In order to minimize an error due to nonuniform irradiation of solution, the sample solutions are diluted to keep the absorbance below 0.1. The error of QY values estimated from the measurements of series of diluted samples at several different excitation wavelengths was around ±12%. PL decay dynamics were measured by using a near IR photomultiplier (R5509-72, Hamamatsu Photonics) and a multi-channel scalar (SR430, Stanford Research). The excitation source was modulated 405 nm light. All the measurements were carried out at room temperature.

## Acknowledgements

## Notes and references

*a* Department of Electrical and Electronic Engineering, Graduate School of Engineering, Kobe University, Rokkodai, Nada, Kobe 657-8501, Japan. E-mail: fujii@eedept.kobe-u.ac.jp

1. G. Konstantatos, I. Howard, A. Fischer, S. Hoogland, J. Clifford, E. Klem, L. Levina, and E. H. Sargent, *Nature*, 2006, **442**, 180–3.

2. S. a McDonald, G. Konstantatos, S. Zhang, P. W. Cyr, E. J. D. Klem, L. Levina, and E. H. Sargent, *Nat. Mater.*, 2005, **4**, 138–42.

3. V. Sukhovatkin, S. Hinds, L. Brzozowski, and E. H. Sargent, *Science*, 2009, **324**, 1542–4.

4. D. V Talapin and C. B. Murray, *Science*, 2005, **310**, 86–9.

5. A. Nag, M. V Kovalenko, J.-S. Lee, W. Liu, B. Spokoyny, and D. V Talapin, *J. Am. Chem. Soc.*, 2011, **133**, 10612–20.

6. J.-S. Lee, M. V Kovalenko, J. Huang, D. S. Chung, and D. V Talapin, *Nat. Nanotechnol.*, 2011, **6**, 348–52.

7. K.-Y. Cheng, R. Anthony, U. R. Kortshagen, and R. J. Holmes, *Nano Lett.*, 2011, **11**, 1952–6.

8. D. Jurbergs, E. Rogojina, L. Mangolini, and U. Kortshagen, *Appl. Phys. Lett.*, 2006, **88**, 233116.

9. J. B. Miller, A. R. Van Sickle, R. J. Anthony, D. M. Kroll, U. R. Kortshagen, and E. K. Hobbie, *ACS Nano*, 2012, **6**, 7389–96.

10. C. M. Hessel, E. J. Henderson, J. G. C. Veinot, V. Uni, R. V February, V. Re, M. Recei, and V. August, *Chem. Mater.*, 2006, 6139–6146.

11. C. M. Hessel, D. Reid, M. G. Panthani, M. R. Rasch, B. W. Goodfellow, J. Wei, H. Fujii, V. Akhavan, and B. A. Korgel, *Chem. Mater.*, 2011.

12. L. M. Wheeler, N. R. Neale, T. Chen, and U. R. Kortshagen, *Nat. Commun.*, 2013, **4**, 2197.

13. Z. C. Holman and U. R. Kortshagen, *Nano Lett.*, 2011, **11**, 2133–6.

14. H. Sugimoto, M. Fujii, K. Imakita, S. Hayashi, and K. Akamatsu, *J. Phys. Chem. C*, 2012, **116**, 17969–17974.

15. H. Sugimoto, M. Fujii, K. Imakita, S. Hayashi, and K. Akamatsu, *J. Phys. Chem. C*, 2013, **117**, 6807–6813.

16. H. Sugimoto, M. Fujii, K. Imakita, S. Hayashi, and K. Akamatsu, *J. Phys. Chem. C*, 2013, **117**, 11850–11857.

17. H. Sugimoto, M. Fujii, Y. Fukuda, K. Imakita, and K. Akamatsu, *Nanoscale*, 2014, **6**, 122–6.

18. G. Lucovsky, *Phys. Rev. B*, 1979, **19**, 2064–2073.

19. B. N. D. Tsu, D. V., G. Lucovsky, *Phys. Rev. B*, 1989, **40**, 1795–1805.

20. X. Pi, L. Mangolini, S. Campbell, and U. Kortshagen, *Phys. Rev. B*, 2007, **75**, 085423.

21. Y. Arai, E.; Nakamura, H.; Terunuma, *J. Electrochem. Soc.*, 1973, 980–987.

22. S. M. A. Durrani, M. F. Al-Kuhaili, and E. E. Khawaja, *J. Phys. Condens. Matter*, 2003, **15**, 8123–.

23. Z. H. Lu, J. P. McCaffrey, B. Brar, G. D. Wilk, R. M. Wallace, L. C. Feldman, and S. P. Tay, *Appl. Phys. Lett.*, 1997, **71**, 2764.

24. S. M. Sze and K. K. Ng, in *Physics of Semiconductor Devices, 3rd Edition.; John Wiley & Sons, Inc.; NJ*, 2007, pp. 164, 682.

25. M. Fujii, H. Sugimoto, M. Hasegawa, and K. Imakita, *J. Appl. Phys.*, 2014, **115**, 084301.

26. M. C. M. Chandrasekhar, H. R. Chandrasekhar, M. Grimsditch, *Phys. Rev. B*, 1980, **22**, 4825–4833.

27. R. C. Newman and R. S. Smith, *Solid State Commun.*, 1967, **5**, 723–726.

28. P. Deak, A. Gali, A. Solyom, P. Ordejon, K. Kamaras, and G. Battistig, *J. Phys. Condens. Matter*, 2003, **15**, 4967–4977.

29. R. Guerra, S. Ossicini, R. Emilia, and P. Morselli, *J. Am. Chem. Soc.*, 2014, **136**, 4404–4409.

30. E. Arai, H. Nakamura, and Y. Terunuma, *J. Electrochem. Soc.*, 1973, **120**, 980–987.

31. M. A. Kessler, T. Ohrdes, B. Wolpensinger, and N.-P. Harder, *Semicond. Sci. Technol.*, 2010, **25**, 055001.

32. F. Iori, E. Degoli, M. Palummo, and S. Ossicini, *Superlattices Microstruct.*, 2008, **44**, 337–347.

33. M. Fujii, Y. Yamaguchi, Y. Takase, K. Ninomiya, and S. Hayashi, *Appl. Phys. Lett.*, 2005, **87**, 211919.

34. M. Fukuda, M. Fujii, and S. Hayashi, *J. Lumin.*, 2011, **131**, 1066–1069.

35. A. van Driel, I. Nikolaev, P. Vergeer, P. Lodahl, D. Vanmaekelbergh, and W. Vos, *Phys. Rev. B*, 2007, **75**, 035329.

36. J. R. Lakowicz, *Principles of fluorescence spectroscopy*, 2006.

*Nanoscale Accepted Manuscript*

**TOC entry**

We present a new route for mass-production of B and P codoped all-inorganic colloidal Si nanocrystals from hydrogen silsesquioxane. The NCs are dispersible in methanol without organic ligands due to the formation of heavily B and P doped hydrophilic shell on the surface of Si NCs.